The Instability of Unsteady Boundary Layers in Porous Media

D.A.S. Rees, A. Selim, and J.P. Ennis-King

1 Introduction

The aim of this Chapter is to summarise the state-of-the-art in the study of the instability of unsteady diffusive boundary layers in porous media. We shall focus on the boundary layer which is formed when the temperature or solute concentration at a plane boundary is changed instantaneously to a new level. Such an idealised system may be applied in a variety of contexts, such as in the subsurface storage of carbon dioxide which is expanded upon below, and it shall be regarded as the standard problem in this Chapter. The thermal/solutal field which then forms is unsteady and it spreads outwards uniformly by diffusion. When the evolving system is unstably stratified, i.e. less dense fluid lies below more dense fluid, it is stable at first but eventually becomes unstable. It is therefore necessary to determine the critical time after which the system is deemed unstable. Many methods have been used to do this and much of the attention here will be focused on describing and comparing these methods. It is hoped that such a discussion will inform and guide future work on the stability of unsteady basic states. We also summarise modifications to this standard problem: isolated disturbances, anisotropy, ramped heating, internal heat sources and local thermal nonequilibrium. Thereafter, we discuss the present

D.A.S. Rees
University of Bath, Bath, UK
e-mail: D.A.S.Rees@bath.ac.uk

A. Selim
University of Bath, Bath, UK

J.P. Ennis-King
Cooperative Research Centre for Greenhouse Gas Technologies,
CSIRO Petroleum, Clayton South,
VIC, Australia

P. Vadász (ed.), *Emerging Topics in Heat and Mass Transfer in Porous Media*,

knowledge on how the growing disturbances are modified when they become large and enter the nonlinear regime. The Chapter ends with a checklist of topics which could usefully be pursued.

2 Background

Although the thermal version of the problem has often been the focus of application e.g. to porous insulation or geothermal systems, there is increasing interest in the unsteady boundary layer due to solute diffusion in the subsurface. For example a fertilizer or a pollutant can dissolve in the water near the ground surface and increase its density. When convection begins, the dissolved substance is carried downwards. A similar phenomenon can occur in the groundwater beneath saline lakes, where evaporation at the surface increases brine density. The migration of brine due to convection has implications for the possible use of salt lakes as disposal sites for pumped saline groundwater (Wooding et al. 1997).

A more recent area of application has arisen from proposals for the large scale subsurface storage of carbon dioxide in order to reduce atmospheric emissions and so limit the effects of hydrocarbon usage on global climate. Typical storage locations would be deeper than 800–1000 m, and at these subsurface conditions the carbon dioxide-rich phase is about half to two-thirds the density of the formation water. After injection into permeable rock beneath a suitable low permeability sealing rock, some of the carbon dioxide will rise due to buoyancy and accumulate beneath the seal. At the same time carbon dioxide dissolves in the formation water (typical solubility is 2–5% by weight depending on salinity). Unusually for a gas, the dissolved carbon dioxide increases the fluid density, and thus the system becomes unstably stratified (Ennis-King and Paterson 2005). The onset of convection significantly accelerates the further dissolution of carbon dioxide, and is important for assessing the security of storage over hundreds or thousands of years.

In these examples of solutal convection, the mapping onto the simplified problem of an instantaneous rise in concentration at a sharp boundary assumes that the initial transport process (e.g. the migration of the gas-phase carbon dioxide) is fast compared with the evolution of the boundary layer. In the carbon dioxide example, there is the additional complication of a two-phase region at the top boundary, which is simplified into a boundary condition of constant solute concentration for a single phase system. The transport properties of typical rocks are neither homogeneous nor isotropic, and indeed the inhomogeneity is present across a wide range of length scales. Thus the standard problem, based on an homogeneous and isotropic porous medium, is only the first step to a theory that can make useful predictions in real contexts.

As a further complication, in many cases the solute can react with the minerals in the rock, altering both permeability and fluid density. This is true of carbon dioxide, which forms a weak acid when dissolved. These alterations can act to either oppose or strengthen convection, depending on whether the geochemical reactions lead to net precipitation or net dissolution. Such coupling goes well beyond the standard problem, but again needs to be assessed in practical applications (Ennis-King and Paterson 2007).

3 Governing Equations

Darcy's law and the Boussinesq approximation are assumed to be valid, the porous medium is taken to be isotropic and rigid, and the fluid and solid phases are taken to be in local thermal equilibrium. Subject to these constraints, the dimensional equations governing flow and the transport of one diffusing species (taken as temperature here) are

$$\frac{\partial \overline{u}}{\partial \overline{x}} + \frac{\partial \overline{v}}{\partial \overline{y}} = 0, \tag{1a}$$

$$\overline{u} = -\frac{K}{\mu}\frac{\partial \overline{P}}{\partial \overline{x}}, \tag{1b}$$

$$\overline{v} = -\frac{K}{\mu}\frac{\partial \overline{P}}{\partial \overline{y}} + \frac{\rho g \beta K}{\mu}(T - T_\infty), \tag{1c}$$

$$\frac{\partial T}{\partial \overline{t}} + \overline{u}\frac{\partial T}{\partial \overline{x}} + \overline{v}\frac{\partial T}{\partial \overline{y}} = \alpha\Big(\frac{\partial^2 T}{\partial \overline{x}^2} + \frac{\partial^2 T}{\partial \overline{y}^2}\Big). \tag{1d}$$

In these equations $\overline{x}$ is the coordinate in the horizontal direction while $\overline{y}$ is vertically upward. The corresponding velocities are $\overline{u}$ and $\overline{v}$, respectively. All the other terms have their usual meaning for porous medium convection: K is the permeability, μ is the dynamic viscosity, ρ is the density of the fluid at the ambient temperature, T_∞. The heated horizontal surface is held at the temperature T_w, where $T_w > T_\infty$. Finally, the quantities g, β and α are gravity, the coefficient of cubical expansion and the thermal diffusivity of the saturated medium, respectively.

Two possible nondimensionalisations may be made depending on whether convection is to take place in a deep-pool system (i.e. a semi-infinite domain) or in a layer of uniform thickness. The former has no natural physical lengthscale while the latter does. In the former case nondimensionalisation takes place using

$$L = \frac{\mu\alpha}{\rho g \beta K (T_w - T_\infty)} \tag{2}$$

as a natural lengthscale based on the properties of the porous medium and the saturating fluid, while, in the latter case, the depth of the layer is taken. Thus there is no Darcy–Rayleigh number for deep pool systems, but there is for the finite thickness layer. Indeed, (2) is equivalent to setting $\mathrm{Ra} = 1$, where $\mathrm{Ra} = \rho g \beta K (T_w - T_\infty) L/\mu\alpha$ is the Darcy–Rayleigh number, and rearranging for L. In this Chapter we consider the deep-pool system as representing our standard system.

On using the scalings,

$$\overline{t} = \frac{L^2}{\alpha}t, \qquad (\overline{x}, \overline{y}) = L(x, y), \qquad (\overline{u}, \overline{v}) = \frac{\alpha}{L}(u, v),$$
$$\overline{P} = \frac{\alpha\mu}{K}p, \qquad T = T_\infty + (T_w - T_\infty)\theta, \tag{3}$$

Equations (1a, b, c, d) become,

$$\frac{\partial u}{\partial x} + \frac{\partial v}{\partial y} = 0, \tag{4a}$$

$$u = -\frac{\partial p}{\partial x}, \tag{4b}$$

$$v = -\frac{\partial p}{\partial y} + \theta, \tag{4c}$$

$$\frac{\partial \theta}{\partial t} + u\frac{\partial \theta}{\partial x} + v\frac{\partial \theta}{\partial y} = \frac{\partial^2 \theta}{\partial x^2} + \frac{\partial^2 \theta}{\partial y^2}. \tag{4d}$$

The boundary conditions corresponding to a sudden change in the boundary temperature are:

$$y = 0: \quad v = 0, \quad \theta = 1 \qquad \text{and} \qquad y \to \infty: \quad v, \theta \to 0, \tag{4e}$$

while $\theta = 0$ everywhere for $t < 0$.

For simplicity we shall treat the problem as two dimensional and adopt the streamfunction in place of the velocities and pressure; we set

$$u = -\frac{\partial \psi}{\partial y} \qquad \text{and} \qquad v = \frac{\partial \psi}{\partial x}, \tag{5}$$

and eliminate pressure by cross-differentiation. Equations (4) reduce to

$$\frac{\partial^2 \psi}{\partial x^2} + \frac{\partial^2 \psi}{\partial y^2} = \frac{\partial \theta}{\partial x}, \tag{6a}$$

$$\frac{\partial \theta}{\partial t} + \frac{\partial \psi}{\partial x}\frac{\partial \theta}{\partial y} - \frac{\partial \psi}{\partial y}\frac{\partial \theta}{\partial x} = \frac{\partial^2 \theta}{\partial x^2} + \frac{\partial^2 \theta}{\partial y^2}, \tag{6b}$$

which are to be solved subject to the boundary conditions,

$$y = 0: \quad \psi = 0, \quad \theta = 1 \qquad \text{and} \qquad y \to \infty: \quad \psi, \theta \to 0, \tag{6c}$$

and the initial condition that

$$\psi = \theta = 0 \quad \text{at} \quad t = 0. \tag{6d}$$

The basic state which we analyse for stability is given by $\psi = 0$, i.e. no flow, and

$$\theta = \operatorname{erfc}(\eta) = \frac{2}{\sqrt{\pi}} \int_\eta^\infty e^{-\xi^2}\, d\xi, \tag{7}$$

where

$$\eta = \frac{y}{2\sqrt{t}}. \tag{8}$$

Thus the basic state is one where the temperature field expands with time, but otherwise keeps the same shape, i.e. it is self-similar.

4 Linearised Stability Equations

Given that the basic thermal profile has uniform thickness in terms of η, it is very reasonable to make a coordinate transformation to take advantage of that fact, and it means that computational grids may then be used efficiently. It is also convenient to modify the time coordinate. Therefore we shall change from an (x, y, t) system to an (x, η, τ) system where

$$\tau = t^{1/2}. \tag{9}$$

In addition, we shall introduce perturbations with amplitude, ϵ, according to

$$\psi = \epsilon\hat{\psi}, \qquad \theta = \operatorname{erfc}\eta + \epsilon\hat{\theta}, \tag{10}$$

where linearised theory is obtained when $\epsilon \ll 1$, while the fully nonlinear perturbation equations are obtained when $\epsilon = 1$. The perturbation equations are, therefore,

$$4\tau\frac{\partial^2\hat{\psi}}{\partial x^2} + \frac{1}{\tau}\frac{\partial^2\hat{\psi}}{\partial\eta^2} = 4\tau\frac{\partial\hat{\theta}}{\partial x}, \tag{11a}$$

$$2\tau\frac{\partial\hat{\theta}}{\partial\tau} + 2\epsilon\tau\Big(\frac{\partial\hat{\psi}}{\partial x}\frac{\partial\hat{\theta}}{\partial\eta} - \frac{\partial\hat{\psi}}{\partial\eta}\frac{\partial\hat{\theta}}{\partial x}\Big) = 4\tau^2\frac{\partial^2\hat{\theta}}{\partial x^2} + \frac{\partial^2\hat{\theta}}{\partial\eta^2} + 2\eta\frac{\partial\hat{\theta}}{\partial\eta} + \frac{4}{\sqrt{\pi}}\,\tau e^{-\eta^2}\frac{\partial\hat{\psi}}{\partial x}. \tag{11b}$$

Small-amplitude roll cell perturbations may be analysed by setting $\epsilon = 0$ in (11) and by substituting,

$$\hat{\psi}(\eta, x, \tau) = \Big[i\Psi(\eta, \tau)e^{ikx} - \text{c.c.}\Big], \tag{12a}$$

$$\hat{\theta}(\eta, x, \tau) = \Big[\Theta(\eta, \tau)e^{ikx} + \text{c.c.}\Big], \tag{12b}$$

where c.c. denotes complex conjugate. The wavenumber of the rolls is k, and therefore their wavelength is $2\pi/k$. The resulting equations for Ψ and Θ are,

$$\Psi'' - 4\tau^2k^2\Psi = 4\tau^2k\Theta, \tag{13a}$$

$$2\tau\Theta_\tau = \Theta'' + 2\eta\Theta' - 4\tau^2k^2\Theta - \frac{4}{\sqrt{\pi}}\,\tau k e^{-\eta^2}\Psi, \tag{13b}$$

where primes denote derivatives with respect to η. The boundary conditions to be satisfied by these disturbances are that

$$\eta = 0: \quad \Psi = \Theta = 0 \qquad \text{and} \qquad \eta \to \infty: \quad \Psi, \Theta \to 0. \tag{13c}$$

5 Comparison of the Methods Used

The overall system given by (13) is parabolic in time which implies that the most natural method of solution is to follow the evolution of disturbances. The other commonly used ways of assessing the stability characteristics are (i) by reducing (13) to an ordinary differential eigenvalue problem for the critical time, (ii) using a local Rayleigh number method which compares the system with the Darcy–Bénard problem and (iii) using an energy method to find the earliest time for which a fully nonlinear disturbance suffers no growth. In this section we shall discuss the merits and demerits of each approach.

5.1 Quasi-Static Analyses

Generally, within the context of boundary layer stability theory, the earliest works reduce the linearised stability equations to ordinary differential form in some way, and then the critical parameter (e.g. Rayleigh number, Reynolds number, time) is obtained as an eigenvalue. More specifically, in the present context, such ordinary differential eigenvalue problems arise by assuming that all time-derivatives are zero—this may be called a quasi-static assumption. Whilst this assumption seems reasonable, it is essential to note that the critical time depends on whether the quasi-static assumption is made before the coordinate transformation (8,9) or afterwards. When it is made beforehand, (13) yield,

$$\Psi'' - 4\tau^2 k^2 \Psi = 4\tau^2 k \Theta, \tag{14a}$$

$$\Theta'' + 2\eta\Theta' - 4\tau^2 k^2 \Theta - \frac{4}{\sqrt{\pi}} \tau k e^{-\eta^2} \Psi = 0. \tag{14b}$$

When it is made afterwards, (14a) remains the same, but (14b) is modified by the removal of the $2\eta\Theta'$ term to give,

$$\Theta'' - 4\tau^2 k^2 \Theta - \frac{4}{\sqrt{\pi}} \tau k e^{-\eta^2} \Psi = 0. \tag{14c}$$

We name these quasi-static cases QS1 and QS2 respectively, and they are known as propagation theory and the frozen time method. Our computed critical values of τ and k are shown in Table 1; these values correspond to the minimum value on the neutral curve.

Table 1 Critical times and wavenumbers for the different methods. QS quasi-static; LR local Rayleigh number; ES energy stability; AT amplitude theory. Results marked with an asterisk are extrapolated from finite thickness calculations

Case	τ_c	t_c	k_c	Reference
QS1	12.9439	167.544	0.06963	Selim and Rees (2007a)
QS2	7.4559	55.590	0.05834	Present chapter
QS3	12.43	154.5	0.0736	Yoon and Choi (1989)
QS4	7.27	52.85	0.07428	Kim et al. (2003)
LR1	46.5520	2261.2	0.06607	Tan et al. (2003)
LR2	9.8696	97.409	0.07958	Present chapter
ES1 *	~ 9.6	~ 93		Caltagirone (1980)
ES2 *	~ 5.5	~ 30		Ennis-King et al. (2005)
AT1	8.9018	79.242	0.07807	Selim and Rees (2007a)
AT2 *	~ 8.9	~ 80		Caltagirone (1980)
AT3a *	8.7	75	0.066	Ennis-King et al. (2005)
AT3b	10.56	111.5	0.0752	Ennis-King et al. (2005)
AT4	12.1	147	0.07	Riaz et al. (2006)
AT5 *	8.671	75.19	0.06529	Xu et al. (2006)
AT6 *	7.75	60	0.05	Hassanzadeh et al. (2006)

It is clear from Table 1 that there is a very substantial difference between the critical times and wavenumbers for cases QS1 and QS2. We believe that it is not at all useful to discuss which case is the correct one, for both are the result of making strong assumptions which are essentially arbitrary. There is no reason to believe that the setting of the time derivative to zero corresponds to the behaviour of a real disturbance. Indeed, it could be argued quite strongly that a zero time derivative is a very strong constraint. The work of Selim and Rees (2007a) shows that disturbances which evolve in time have profiles which vary in shape, and, in particular, they become thinner in terms of η (but thicker, in terms of y) with time. Therefore the magnitude of Θ at any chosen value of η (or y) evolves at a different rate from the value of Θ at any other chosen value of the coordinate. Thus the quasi-static method puts a strong constraint on which disturbances are allowable.

In addition to the critical values differing greatly, the onset profiles (not shown due to the need for brevity) are also very different. The presence of the $2\eta\Theta'$ term for the QS1 case causes a superexponential decay in the temperature field, as opposed to an exponential one for the QS2 case. The QS1 disturbance is much narrower than the QS2 disturbance.

Two other chapters offer quasi-static results for the identical problem. Yoon and Choi (1989) consider a finite layer, and when the Rayleigh number is large, the deep-pool results are obtained. They approximated the complementary error function solution given in (7) by a fourth order polynomial in η, and employ propagation theory. Their critical data are labelled as QS3 in Table 1 and they are close to those of QS1, which is also a propagation theory analysis, but one which is based on the precise basic temperature profile. The second chapter is by Kim et al. (2003); these authors employ a propagation theory using v and θ as the dependent variables. However, they apply the boundary condition, $\partial v/\partial y = 0$, on the lower surface and it is termed a stress free condition. Given the equation of continuity, (4a), this implies that $\partial u/\partial x = 0$ on $x = 0$, and hence that u is a constant. It is not clear how such a condition may be interpreted, but certainly their critical data, labelled QS4, are very different from those of cases QS1 and QS3 as the boundary condition used is quite different.

Finally, we mention the use of a subtle technical detail in the chapters by Yoon and Choi (1989) and Kim et al. (2002, 2003). In these chapters the disturbances are assigned particular forms of variation with time prior to the setting of all time derivatives to zero. All three of these chapters develop their linearised stability equations using the vertical velocity instead of the streamfunction. On scaling grounds they set the vertical velocity to be proportional to t, but the equation for the vertical velocity has a similar form to (13a) above by having no time derivative. Therefore such a rescaling has no effect on the computed critical values, and their propagation theory stability criteria are identical to that which would be obtained without using the scaling. But we note that, should an analogous clear fluid problem be considered, or even a porous medium system where the velocity time derivative is not negligible, then such scalings will alter the stability criteria.

5.2 Local Rayleigh Number Analysis

This is a 'quick and easy' approach to finding the rough values of the critical parameters. Therefore it may be used to provide a rapid estimate prior to using more sophisticated techniques. In essence the method derives an expression for a time-dependent Rayleigh number and compares this with the classical value of $4\pi^2$, which corresponds to Darcy–Bénard convection in a horizontal layer of uniform thickness (see Lapwood 1948, Horton and Rogers 1945). In addition, the nondimensional wavenumber is set equal to π, which is the critical Darcy–Bénard wavenumber.

The thickness of the thermal layer we are considering grows in time, and therefore a Rayleigh number which is based upon that thickness will also increase. The chief issue, then, is how to define the thickness of the thermal layer. Tan et al. (2003) used the following as the local Rayleigh number,

$$\mathrm{Ra}_{\mathrm{Tan}} = -\frac{\rho g \beta K}{\mu\alpha}\Big(\hat{y}^2\frac{\partial T}{\partial \hat{y}}\Big), \tag{15}$$

so that this function depends on both $\hat{y}$ and $\hat{t}$, which, we note, are dimensional quantities. After the expression for the dimensional basic temperature field is substituted into (15), $\mathrm{Ra}_{\mathrm{Tan}}$ is maximised over $\hat{y}$ to find its largest value at any point in time. The maximising value of $\hat{y}$ is then taken as the thickness of the layer: $\hat{y}_c = 2\sqrt{\alpha\hat{t}}$. In terms of the present nondimensionalisation, we obtain

$$\mathrm{Ra}_{\mathrm{Tan,max}} = \frac{\rho g \beta K(T_w - T_\infty)}{\mu\alpha}\frac{4\sqrt{\alpha\hat{t}}}{e\sqrt{\pi}} = \Big(\frac{4}{e\sqrt{\pi}}\Big)\tau. \tag{16}$$

On setting this equal to $4\pi^2$ we obtain the critical time,

$$\tau_c = \pi^{5/2} e, \tag{17}$$

which is given numerically in Table 1 as case LR1. This value is very different from the quasi-static values, being roughly a factor of 4 times as large as for the other methods. On the other hand, the dimensional wavelength of the cells may be taken as being $2\hat{y}_c$, since Darcy–Bénard convection has cells of square cross-section as its most unstable mode, and this translates into

$$k_c = \frac{2\pi L}{2\hat{y}_c} = \frac{1}{\pi^{3/2} e}, \tag{18}$$

which is also given in Table 1. This value is quite close to those obtained by other methods.

An alternative and less complicated approach would be to say that the boundary layer thickness in terms of η is 2, and that a local Rayleigh number could be defined according to

$$\mathrm{Ra}_{\mathrm{local}} = \frac{\rho g \beta K (T_w - T_\infty)\hat{y}_{\mathrm{bl}}}{\mu\alpha}, \tag{19}$$

which varies only in time. The boundary layer thickness in terms of $\hat{y}$ is given by

$$\eta_{\mathrm{bl}} = \frac{\hat{y}_{\mathrm{bl}}}{2\sqrt{\alpha\hat{t}}} = 2, \tag{20}$$

and therefore $\hat{y}_{\mathrm{bl}} = 4\sqrt{\alpha\hat{t}}$. The setting of the Rayleigh number given in (19) to $4\pi^2$ for this value of y_{bl} yields,

$$\tau_c = \pi^2. \tag{21}$$

The corresponding wavenumber becomes,

$$k_c = \frac{1}{4\pi}. \tag{22}$$

These values are also placed in Table 1 for comparison, and are denoted as case LR2.

Admittedly, these are only two possible choices, but they seem to indicate that the critical wavenumber is not so highly affected by different ways of defining the boundary layer thickness or the way in which a local Rayleigh number number is chosen. However, the critical time is affected strongly. Given that there is no definitive way of choosing an expression for the local Rayleigh number, we would conclude that this method is only capable of providing a very rough ball-park estimate of the critical time and wavenumber prior to the use of more accurate methods.

5.3 Energy Stability Analysis

The idea behind this method is to find a time before which no disturbances grow. An energy functional is defined:

$$\bar{\Theta} = \langle \Theta^2 \rangle^{1/2} = \Big[\int_0^\infty \Theta^2 \, dy \Big]^{1/2}, \tag{23}$$

and variational methods are used to determine the earliest time for which

$$\frac{\mathrm{d}\bar{\Theta}}{\mathrm{d}t} = 0. \tag{24}$$

Caltagirone (1980) applied this technique to the finite layer. His result for the deep-pool system, which may be extrapolated from his large-Rayleigh number result, is given in Table 1 and labelled as case ES1. A second analysis of this type, extending Caltagirone's work to anisotropic media, was undertaken by Ennis-King et al. (2005), but their isotropic results (labelled ES2 in Table 1) are somewhat at variance with those of Caltagirone by suggesting a much earlier critical time. An independent third study by Xu et al. (2006) undertakes an identical anisotropic analysis to that of Ennis-King et al. (2005) and they present a graph for the critical Rayleigh number against time. However, there is insufficent information within that chapter to allow us to determine which, if either, of the energy stability analyses of Caltagirone (1980) and Ennis-King et al. (2005) is correct.

There is a widely held belief that energy methods always yield the definitive smallest parameter. In the present context Caltagirone's critical time is much closer to those using an accurate amplitude theory (described in the next subsection), but his computed critical time using amplitude theory is lower than that for energy stability theory. The critical times obtained by Ennis-King et al. (2005) are such that the energy stability analysis yields a earlier critical time than their amplitude theory. Therefore it is clear that the energy stability analysis must be revisited in order to clarify the situation. Some further comments are made on this towards the end of the next subsection.

5.4 Amplitude Theory

This method utilises solutions of the full parabolic disturbance equations, such as those given by (13). As the temperature equation has a single time derivative, it is necessary to provide an initial condition, which is the initial perturbation whose evolution will then be determined. Generally this has been undertaken using either Galerkin methods for a finite thickness layer (Caltagirone 1980, Ennis-King et al. 2005, Xu et al. 2006), or in the deep-pool system by Galerkin methods (Ennis-King et al. 2005) or by finite difference methods (Selim and Rees 2007a). A means of determining the amplitude of the evolving perturbation also has to be defined, and this is not easy to resolve a priori. The options which have been used in the literature are the following: (i) the maximum value of Θ, (ii) the rate of heat transfer at the surface, (iii) a thermal energy content integral, $\langle\Theta\rangle$, and (iv) an 'energy' integral similar to that given in (23). In all cases the chosen measure is evaluated at each timestep and the times at which time-derivative is zero are noted together with the wavenumber, k.

The evolution of $E = \langle\Theta\rangle$ (measure (iii)) for a set of wavenumbers, k, is shown in Fig. 1. These curves are typical of the other measures of the amplitude of the disturbance, which show only quantitative differences. The initial disturbance profile is $\Theta = \eta e^{-3\eta}$ and it was introduced at $\tau = 1$, which is well before the critical time. It is clear that the disturbance decays substantially at first, followed by growth. At later times, the disturbance eventually decays once more, indicating that there is only a finite interval during which growth may take place.

After a suitable number of simulations, a neutral curve may be constructed showing how the onset time varies with wavenumber. This is illustrated in Fig. 2, which displays the neutral curves obtained by Selim and Rees (2007a) corresponding to the first three of the above measures, and to the quasi-static theory. Of the various measures displayed there, the one with the lowest critical time is the thermal energy content measure, which, given that it is an integral, is a global quantity, rather than a local one as represented by the surface rate of heat transfer. This minimum is given in Table 1 and is denoted as case AT1.

The aforementioned chapter by Caltagirone (1980) also presents the results of a full unsteady simulation, the critical values for which are given in Table 1 and denoted by AT2. Apart from the numerical method used, the only difference between his simulation and that of Rees and Selim (2007a) is that his critical values are based on the evolution of $\bar{\Theta} = \langle\Theta^2\rangle^{1/2}$. Despite this difference, the agreement is very good indeed.

Ennis-King et al. (2005) apply Caltagirone's method to both the finite thickness and deep-pool systems, using different sets of basis functions in each case. These result are respectively denoted as case AT3a and AT3b in Table 1 (the AT3b results were not explicitly given in the chapter, but are provided here for comparison).

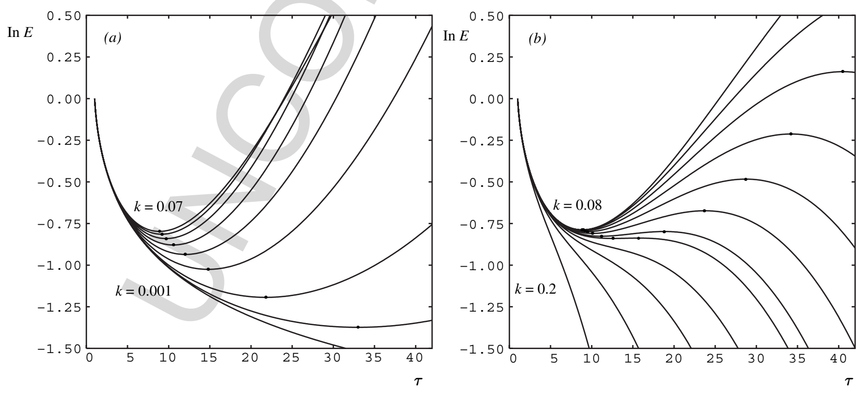

Fig. 1 Variation of $\ln E$ against τ for different values of k

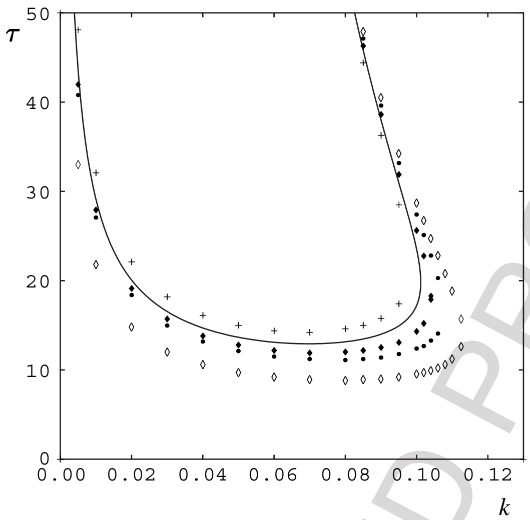

Fig. 2 *Neutral curves*: The continuous curve represents quasi-static theory. The symbol ⋄ represents the thermal energy content. The symbols • and + represent the surface heat flux criterion in terms of η and y respectively. The symbol ⧫ represents the maximum temperature criterion

Again for AT3a there is an extrapolation of the finite depth results to the deep-pool limit, which causes some loss of precision. The AT3b deep-pool results are only weakly dependent on the initial conditions as long as the starting disturbance is within the diffusion layer. The difference between the results in AT3a and AT3b appears to originate from the choice of basis functions and the form of the initial disturbance in each case.

On the other hand, Riaz et al. (2006) used a different set of Galerkin expansion functions in η to obtain a critical time and wavenumber (case AT4) which are quite close to the QS1 case of Selim and Rees (2007a). The analysis of Xu et al. (2006), denoted as case AT5, follows the methodology of Ennis-King et al. (2005) and is an extrapolation of finite thickness results. Thus AT3a and AT5 agree, and give results that are very similar to case AT1 of Selim and Rees (2007a).

The work of Hassanzadeh et al. (2006) (case AT6) uses the same methodology as Ennis-King et al. (2005) and Xu et al. (2006) for the finite thickness case, but varies the type of initial conditions (white noise, or one of two Fourier modes) and the boundary conditions. The lower bound given for the instability corresponds to the zero time derivative condition. The value for t_c is somewhat lower than the corresponding AT3a and AT5 results using a similar approach—the difference may relate to the variation of initial conditions.

5.4.1 Comment on Stability Criteria

Caltagirone (1980), together with many later authors including Kim and Kim (2005) and Kim et al. (2002) who look at slightly different impulsive problems, presents two different stability criteria using amplification theory. One of these is the zero time derivative criterion, $d\bar{\Theta}/dt = 0$, while the other is the time taken for the disturbance to achieve its original value of $\bar{\Theta}$. Kim et al. (2003) go further and say that experimental considerations should be heeded to determine the level of amplification required for marginal stability to be declared. Although Fig. 1 shows the variation of $\langle\Theta\rangle$, it is clear that the latter criterion will yield greatly different critical times depending on when the disturbance is seeded into the boundary layer. Therefore we regard the former criterion as being more intuitive.

5.4.2 Comment on the Choice of Initial Disturbance Profile

The manner in which the initial perturbation profile for the numerical simulations is chosen has been questioned by Kim et al. (2002) who state, quite reasonably, that it is arbitrary. Indeed, it was this fact that motivated the general analysis of Green (1990) who developed a method involving a series expansion about the critical time, where the mode calculated was the result of minimising the critical time over mode shapes (using a Fourier expansion) and the wavenumber, and is such that the growth rate is zero. His method was applied to a problem of ramp heating, and to date it is unknown how good it is for the problem being discussed in this section. However, one of the important conclusions of the work of Selim and Rees (2007a) is that the profile of the initial disturbance generally has very little effect on the critical time whenever the time at which it is introduced into the system is sufficiently early. In other words, all disturbances appear to be attracted towards a common evolutionary path, as shown in Fig. 3, and if the introduction time is sufficiently early, then this process is essentially complete by the time marginal instability occurs.

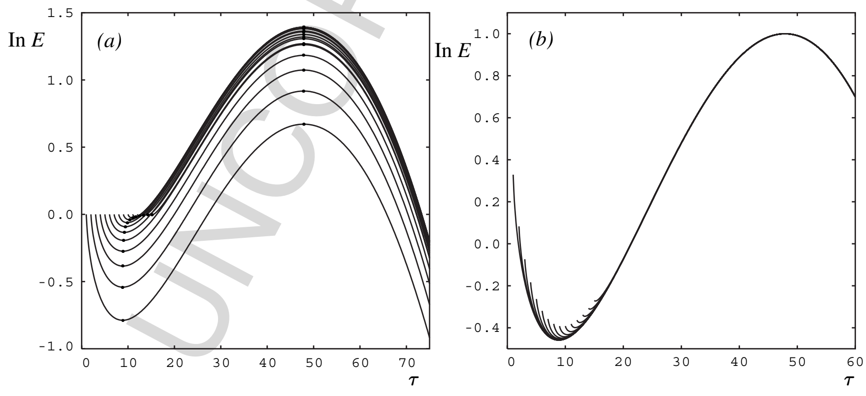

Fig. 3 Variation of ln E against τ for disturbances introduced at various values of τ, for $k = 0.085$. (**a**) Computed ln E curves; (**b**) Normalised ln E curves

5.5 Discussion

What is to be made of the widely differing values of the critical times quoted in Table 1? Energy methods are generally held in high esteem, especially for problems where the basic state whose stability characteristics are being sought is steady. Here we have two sets of results which are very different from one another, and without considering the results obtained by other methods, we are not in a position to decide between them. Both the local Rayleigh number and the quasi-static theories are very definitely approximate, the former more so than the latter. It is certainly possible to calibrate the local Rayleigh number method a posteriori to get an exact match with almost any result we wish, but ideally we need to obtain good results independently of such calibration. The amplitude theory results should be excellent in the sense that the exact linearised equations are being solved. But one also has to consider which is the best way to measure the amplitude of the evolving disturbance—Fig. 2 depicts the different neutral curves corresponding to four such measures, and no doubt the use of $\bar{\Theta}$, defined in (23), would provide a fifth. The numerical results of Ennis-King et al. (2005) for amplitude theory and finite thickness use between 8 and 16 terms in the Galerkin expansion to the full profile of the evolving disturbances, and the comparable results of Xu et al. (2006) have similar accuracy; both are close to those of Caltagirone (1980) and Selim and Rees (2007a). The amplitude results of Ennis-King et al. (2005) for the semi-infinite case, using at least 10 terms in a Galerkin expansion, are close to Selim and Rees (2007a) for k_c but give a larger value for t_c, while the one-term approximation of Riaz et al. (2006) gives a still higher value of t_c.

We would tentatively suggest, therefore, that Caltagirone (1980) and Selim and Rees (2007a) presently give the benchmark critical values for situations where the evolution of disturbances is undertaken. We await confirmation of a further study using energy methods in order to decide between the quoted results of Caltagirone (1980) and Ennis-King et al. (2005). Although we think it likely that such an analysis will provide an earlier critical time than does amplitude theory, it is our belief that the critical profile will not be one that is on the attracting solution path mentioned earlier.

Finally, if we consider the shape of the various neutral curves in Fig. 2, it is worthy of note that each one is quite flat near its minimum, and therefore it is perhaps not surprising that the various methods have yielded quite different critical wavenumbers.

6 Isolated Small-Amplitude Disturbances

In all of the above considerations it has been assumed that the disturbances have been characterised by a single wavenumber in the x-direction and are therefore monochromatic. Should a spatially non-periodic initial disturbance need to be considered, then it is possible to Fourier-transform the disturbance, compute as many single-wavenumber solutions as is required, then apply the inverse Fourier

Transform formula to obtain the resulting evolution of the time-dependent system. Thus it would appear that little else needs to be said about the linear stability problem.

However, there is much interest in the published literature on how localised disturbances evolve. Despite the above statement that a sufficiently early introduction of a disturbance causes the stability criterion to be independent of the disturbance profile, this is true only in terms of its profile in the η-direction. When the disturbance is localised in the x-direction, then it takes time for the disturbance to diffuse horizontally and generate new cells either side of itself.

This process is illustrated in Fig. 4. A full two-dimensional finite difference scheme was used to investigate the evolution of a narrow isolated disturbance placed at $x = 0$. Suitable symmetry conditions were applied at $x = 0$ to mimic correctly the solution in $x < 0$. The Figure shows the boundaries between the thermal cells, i.e. it indicates where there is zero rate of heat transfer. As each boundary is crossed, the sign of the rate of heat transfer changes. The Figure does not indicate the variation of the amplitude of the disturbance, but successive maxima and minima reduce in size as x increases for any chosen τ.

The chief interest here lies in the fact that the wavelength of cells is not uniform. Each new cell that is generated tends to have a larger width than the cell immediately next to it, and each cell tends to grow in width as τ increases. This behaviour is different from that obtained in the analogous situation in Darcy-Bénard convection where unpublished computations undertaken by one of the authors show that cells remain of constant wavelength as they spread into the external undisturbed regions. In the present case, the fastest growing disturbance at any point in time

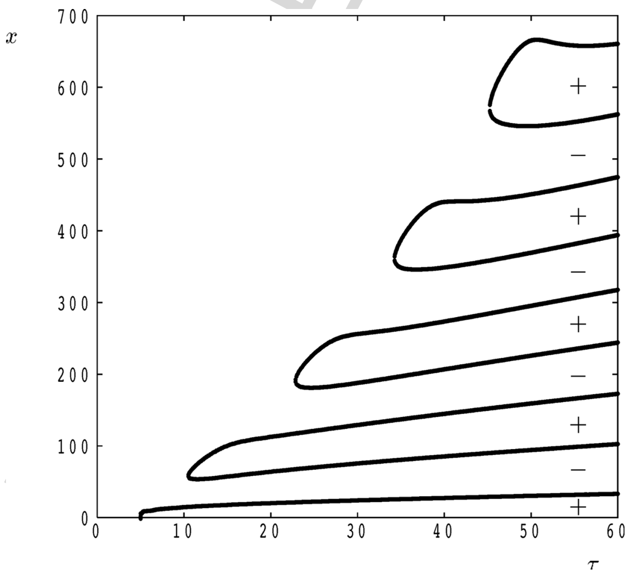

Fig. 4 Depicting the evolution and spread of thermal cell boundaries as τ increases

January 31, 2008 Time: 10:45pm t1-v1.3

has a wavenumber which decreases as time progresses. Therefore we think that the increase in the wavelength is very likely to be related to the fact that smaller wavenumbers grow faster.

7 Other Linear Systems

We now give a quick overview of similar systems considered by various authors. In all cases they will have used one or more of the methods discussed above.

7.1 Anisotropy

Ennis-King et al. (2005) have extended the standard case to include anisotropy in the permeability. The permeability tensor remains diagonal, and so the principle axes remain in the coordinate directions. These authors consider both finite layers and semi-infinite deep-pool systems, employing different nondimensionalisations for the two cases. For the finite layer two different boundary conditions are considered on the unsalted boundary. Energy stability theory and amplitude theory are presented. The change in the isotropic results which are obtained when anisotropy is introduced are much as expected, and are qualitatively identical to the isotropic case. Of most interest is the fact that their results are substantially different from those of Caltagirone (1980) when the porous medium is isotropic, as discussed above.

7.2 Ramped Heating

Kim and Kim (2005) considered a finite layer which is at a uniform temperature initially, but where the temperature of the lower boundary increases linearly with time. They use a Galerkin-based amplitude theory, monitoring the rate of growth of disturbances using $\bar{\Theta}$. Neutral curves are presented which correspond to the criteria $\bar{\Theta}_t = 0$ and $\Theta = 1$ (where $\Theta = 1$ is set at the time the disturbance is introduced). The former they call the 'intrinsic' stability criterion, while the latter is termed the 'marginal' stability criterion. The general tenor of other chapters, and the view of the present authors, is that the former should be called the marginal stability criterion, while the latter is irrelevant, as discussed earlier. The authors state that disturbances grow superexponentially after the 'marginal' stability time; Fig. 1 shows that this is not true for the present standard problem and quite obviously so for values of k close to 0.1 where there is only a small interval of growth before decay is re-established.

Hassanzadeh et al. (2006) also consider a case in which the solute concentration at the boundary decreases linearly with time. This is relevant to underground storage of carbon dioxide, where the pressure in the gas phase may decline and thus reduce the concentration of dissolved carbon dioxide in the two-phase region (although in practice this reduction would not be linear in the pressure at typical conditions of interest). It is shown that for layers of finite thickness and small Rayleigh numbers, a fast enough decrease at the boundary may prevent a perturbation from growing and eliminate convection, whereas in the deep pool limit (large Rayleigh numbers) the instability criterion is unaffected.

7.3 Internal Heat Sources

Kim et al. (2002) also considered a finite layer at a uniform temperature initially. At $t = 0$ a uniform internal heat generation is turned on, which forms an unstably stratified boundary layer at the cold upper surface. This configuration eventually tends to a steady state. Therefore all interest is focussed on the onset times for those cases where the Rayleigh number is above the critical value for the steady state situation. The authors use a propagation/quasi-static theory to determine the onset times—this is performed in terms of the η-variable—and use a quasi-static theory in the Cartesian variables (termed a frozen-time theory). The results obtained by means of these theories differ from one another, but are much closer to one another than are those given by QS1 and QS2 in Table 1.

7.4 Local Thermal Nonequilibrium

Nouri-Borujerdi et al. (2007) modified the standard problem by dropping the assumption that the fluid and solid phases are in local thermal equilibrium. The great majority of chapters reporting convection in porous media assume that the temperatures of the phases are identical locally, that is, they assume that the heat transfer which takes place between the phases either happens so quickly, or else, the flow rate is sufficiently slow, that, to a good approximation, the two-phase system may be described by a single energy equation. But there are situations when such an assumption is not accurate, and then the temperature fields of the two phases have to be modelled by separate, but coupled, equations. The coupling takes the form of source/sink terms that are proportional to the local difference in temperature between the phases, and which allow the flow of heat between the phases.

These authors followed the methodology of Selim and Rees (2007a) by applying a quasi-static theory and an amplitude theory based on $E = \langle \Theta \rangle$. Generally it was found that the critical time decreases as the degree of local thermal nonequilibrium increases. This may be attributed to the fact that the convecting fluid does not have to impart heat to the solid phase, and therefore it experiences less of what might be termed a thermal drag.

8 Nonlinear Studies

Once an evolving disturbance becomes sufficiently strong, it will interact with itself via the nonlinear terms in the governing equations. This will serve to modify the further development of the disturbance in a wide variety of ways. Moreover, the effect of having multiple disturbances (which are distinguished by having different wavenumbers) complicates the situation substantially in terms of their nonlinear interaction.

The earliest nonlinear simulations were undertaken by Elder (1967, 1968). He employed a two-dimensional fully numerical scheme to determine the convection in a finite thickness layer subjected to an instantaneous rise in the temperature of the lower surface. In these simulations, the nondimensional lower boundary temperature was set to $\theta = 1 + \epsilon'(x)$, where ϵ' is a random variable with zero mean. This type of boundary condition provides an alternative means of disturbing the evolving thermal boundary layer. His simulations showed the formation of a highly irregular series of cells within the boundary layer. These interact in a complex manner with cell-merging taking place. Eventually the evolving basic state tends towards a steady linear profile, and there follows a long period of adjustment of the cells. He also considered convection in a fully infinite domain where the initial condition for the basic state is that $\theta = 0$ in $y > 0$ and $\theta = 1$ in $y < 0$.

Caltagirone (1980) also employed a nonlinear finite difference model, but this was used to provide confirmation of his energy theory results.

Selim and Rees (2007b) solved the full two-dimensional equations for the disturbances, but used a horizontal Fourier decomposition together with a vertical finite difference method. Thus the following substitutions were made in (11) where $\epsilon = 1$ was chosen:

$$\psi(x, \eta, \tau) = \sum_{n=1}^{N} \psi_n(\eta, \tau) \sin nkx, \tag{25a}$$

$$\theta(x, \eta, \tau) = \tfrac{1}{2}\theta_0(\eta, \tau) + \sum_{n=1}^{N} \theta_n(\eta, \tau) \cos nkx, \tag{25b}$$

where $N = 5$ was generally found to provide excellent accuracy. The resulting unsteady equations were solved using a variant of the Keller box method, and the initial disturbance took the form,

$$\theta_1 = A_1 \eta e^{-3\eta}, \tag{26}$$

with all other terms in (25) set to zero. The chief qualitative result of this chapter is that strongly nonlinear disturbances suffer from premature stabilisation. The linear stability curves displayed in Fig. 2 indicate that small-amplitude disturbances have only a finite interval of time over which they can grow. The computations of Selim and Rees (2007b) show that restabilisation often takes place earlier than would be expected from the data represented in Fig. 2. Figure 5 shows the evolution of the surface rate of heat transfer of the primary mode,

$$q_1 = \frac{\partial \theta_1}{\partial \eta}\bigg|_{\eta=0}, \tag{27}$$

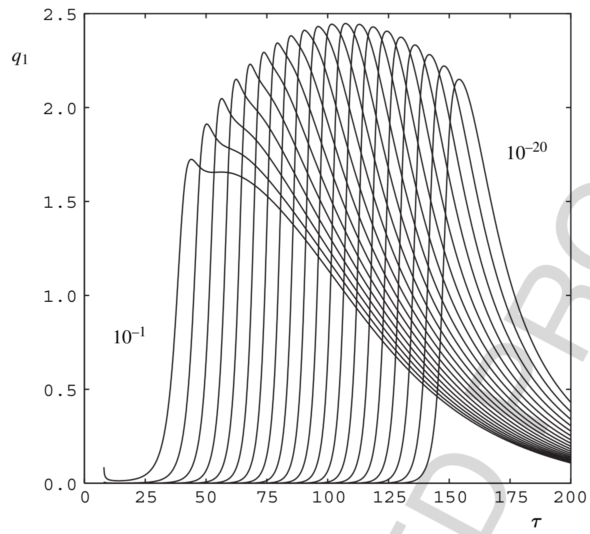

Fig. 5 The variation with τ of q_1 for $k = 0.04$, the disturbance initiation time, $\tau = 8$, and for the amplitudes $A_1 = 10^{-1}, 10^{-2}, \ldots, 10^{-20}$. The curve on the extreme left corresponds to $A_1 = 10^{-1}$ (Selim and Rees 2007b)

for $k = 0.04$ and for a variety of initial amplitudes, A_1. Various features stand out from this Figure. The first is that the time at which restabilisation occurs (defined now as being when q_1 begins to decrease) depends very strongly on the value of A_1. For very small amplitudes the restabilisation time is consistent with linear theory based on a heat transfer criterion. For large amplitudes restabilisation occurs very early indeed. The second feature is that the maximum response does not correspond to the largest initial disturbance amplitude. For this wavenumber, the maximum response occurs when $A_1 \simeq 10^{-12}$.

A third feature is that all disturbances, even in the nonlinear regime, eventually decay towards zero. This is surprising from the point of view that the Rayleigh number based upon the basic boundary layer thickness continues to increase, thereby rendering the boundary layer increasingly unstable. Therefore the solutions shown in Fig. 5 must become unstable to other disturbances. Given that the boundary layer thickens with time, and that convection cells usually tend to a roughly square cross-section, it seems reasonable to attempt to destabilise solutions such as those shown in Fig. 5 using longer wavelength/smaller wavenumber perturbations.

It is this observation which motivated the work contained in Selim and Rees (2007c), who consider subharmonic destabilisations. These authors also used (25), but, for a 2:1 subharmonic case, the primary mode is now taken to correspond to $n = 2$, while the subharmonic corresponds to $n = 1$. In addition, a much larger value of N is taken than for the simulations reported in Selim and Rees (2007b). Typically the magnitude of A_1 is much less than that of A_2, so that the primary

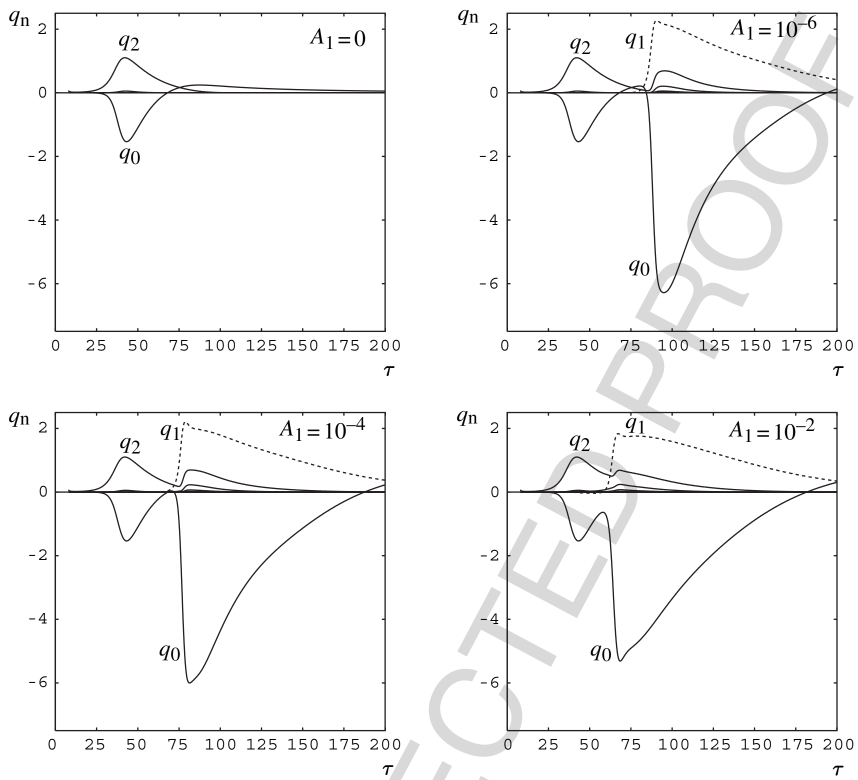

Fig. 6 Variation with τ of the surface rates of heat transfer, q_n, corresponding to the modes, $n = 0, 1, 2, \cdots$. These simulations correspond to $k = 0.035$ and $A_2 = 10^{-1}$. The disturbance was introduced at $\tau = 8$ (from Selim and Rees 2007c)

mode may evolve in almost exactly the same way as before, but, soon after the primary begins to decay, the subharmonic begins to grow and eventually takes over as the dominant pattern.

Figure 6 shows the manner in which the surface rates of heat transfer of each mode vary in time where the primary mode has wavenumber 0.07 and $A_2 = 0.1$. The datum case with no subharmonic disturbance corresponds to $A_1 = 0$, and this exhibits a moderate amount of growth prior to eventual decay. Of particular interest in the other subfigures are the times at which the subharmonic, shown by the q_1 curves, takes over as the dominant pattern. As might be expected, the larger the initial value of A_1, the earlier this happens. Once more, it is interesting to note that the largest magnitude in the mean rate of heat transfer, q_0, for the cases we present, is obtained for the smallest value of A_1, rather than for the largest.

Contours of the temperature disturbance field at various times are shown in Fig. 7 to illustrate the manner in which the subharmonic destabilisation takes place. At $\tau = 10$ an apparently uniform set of cells is present. For convenience we shall label

January 31, 2008 Time: 10:45pm t1-v1.3

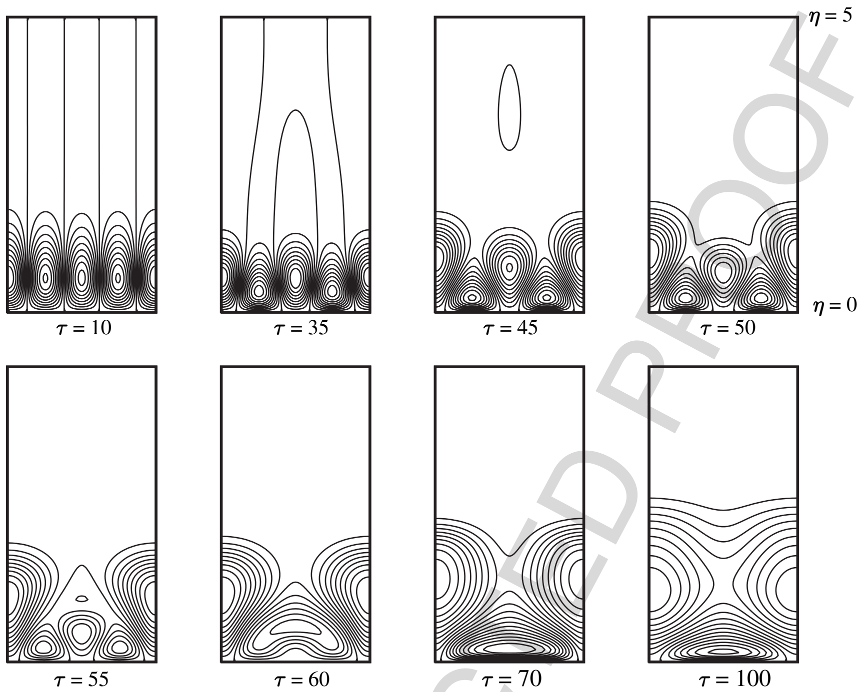

Fig. 7 Contours of the perturbation temperature field at chosen times for the subharmonic instability corresponding to $k = 0.035$, $A_1 = 10^{-2}$ and $A_2 = 10^{-1}$, where the disturbance was introduced at $\tau = 8$ (from Selim and Rees 2007c)

these cells 0 through to 4 from left to right, noting that cells 0 and 4 are identical. The subharmonic instability now manifests itself by causing (i) even numbered cells to become stronger and occupy more space in the η-direction than do the odd numbered cells, and (ii) cells 0 and 4 become stronger than cell 2. Once $\tau = 55$ is reached, cells 0 and 4 are now dominant, with the remains of cells 1, 2 and 3 occupying a triangular-shaped region corresponding to the contour $\Theta = 0$. After this point, cells 1 and 3 merge, destroying cell 2 in the process. Thereafter the fully developed nonlinear subharmonic convection is fully established. We note that the final subfigure, which corresponds to $\tau = 100$, has the following features: (i) the middle cell is pushed close to the heated surface due to a strong inflow towards the surface and (ii) the outer cells have expanded substantially due to the fact that the flow is away from the surface.

A full categorisation of the roles played by the sizes of A_1 and A_2 is quite a large task, especially as such a systematic set of computations would need to take place over a set of wavenumbers. Moreover, other subharmonic disturbances may also be considered, such as 1:3, 2:3 and 3:4, where cases of the form $M{:}M+1$ may be regarded as being very much like the well-known Eckhaus instability.

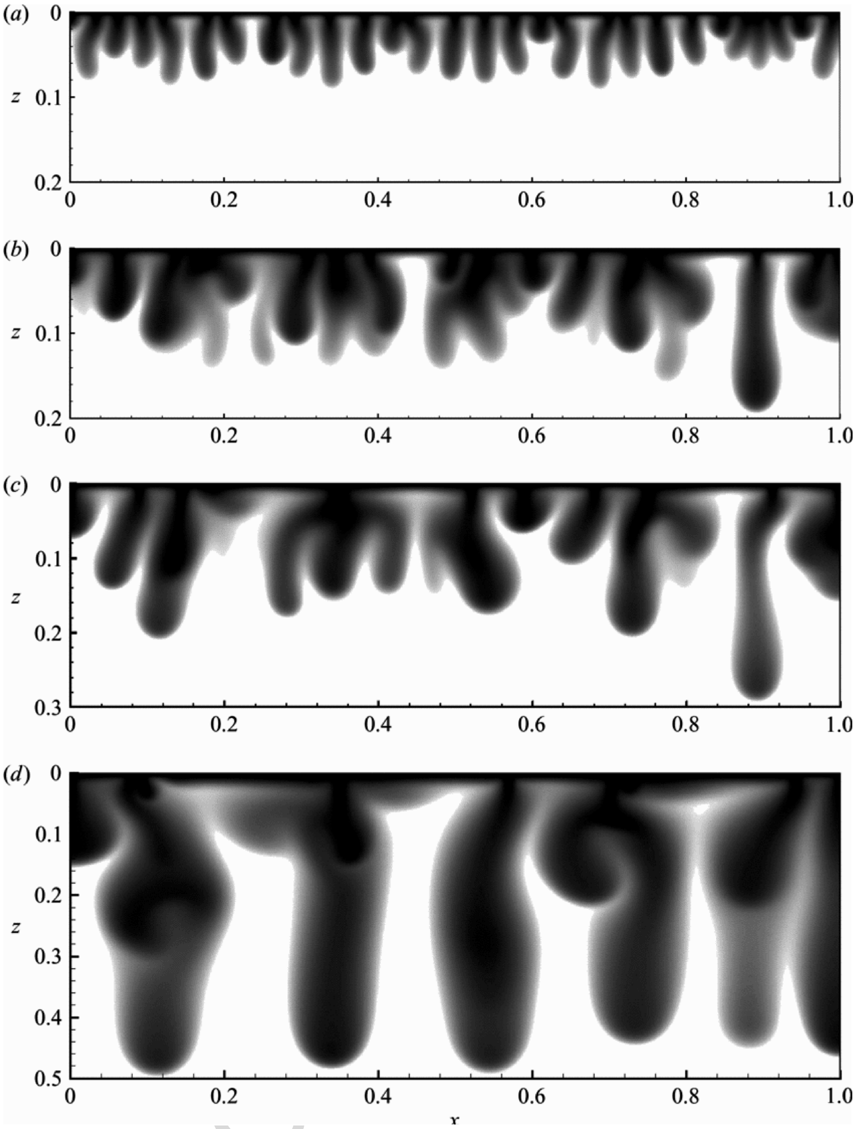

Fig. 8 Contours of concentration showing the change in the wavelength of plumes with time. For unit vertical depth and Ra $= 4000$: (**a**) $t = 1$, (**b**) $t = 1.8$, (**c**) $t = 2.3$ and (**d**) $t = 3.8$ (Riaz et al. 2006)

Given that Fig. 6 also shows that the subharmonic itself decays after a certain time, it suggests the possibility of a further subharmonic destabilisation. However, it is important to realise that the use of a horizontal Fourier expansion by Selim and Rees (2007b, c) is a very strong constraint on the overall behaviour of the system. Various chapters have appeared which use finite difference methods to solve systems such as the present one, but with large horizontal physical domains, and whilst the fact that a finite domain is also a constraint, it is nevertheless a very much weaker one. These chapters suggest that the true physical behaviour is one where the flow becomes chaotic. The first hint of this is in the FLUENT computations of Tan et al. (2003) who solve the full two-dimensional equations of motion in Cartesian coordinates in a fairly small region. No mention is made of how disturbances are introduced into the system, but waves of uniform wavelength appear. However, one of these is stronger than the others and begins to grow preferentially, which bypasses the subharmonic cascade of Selim and Rees (2007c). A similar scenario was found by Riaz et al. (2006) who considered a system with a very much larger aspect ratio.

The work of Riaz et al. (2006) concentrates to a large extent on the postcritical dynamics when the instabilities have become strongly nonlinear. There is too much detailed information in their chapter for it to be summarised briefly here, and we restrict attention to the flow shown in Fig. 8. These authors consider convection due to the sudden introduction of a solute at the upper surface of a layer of finite depth. The simulation shown used $\mathrm{Ra} = 4000$ and the snapshots shown are at times which are sufficiently early that the lower surface has not affected the development of the instability. Figure 8 shows an essentially chaotic system where the observed wavelength clearly increases with time. Presumably this is not a continuous increase, but rather it comes about by the nonlinear interactions of embryonic plumes especially the merging of neighbouring plumes. In this regard, the subharmonic cascade of Selim and Rees (2007c) could be regarded as providing part of the explanation of this. But equally well, the merging of two plumes could also be regarded as a form of Coandă effect (where a jet of fluid is deflected towards a neighbouring surface). Here, by analogy, the lack of availability of fluid to entrain from one side of a plume causes the deflection of the plume in that direction, and therefore it is natural for two plumes to move toward one another and to coalesce.

Other features arise if the suddenly heated/salted surface is semi-infinite, as the leading edge of the surface then plays a strong role, at least initially. Although the primary aim of the chapter by Rees and Bassom (1993) is the description of the instability of a steady thermal boundary layer generated by a semi-infinite heated surface, these authors also presented a computation of the immediate aftermath of the sudden rise of the surface temperature. One snapshot of this process is shown in Fig. 9 where multiple cells have been generated, but which have also been ejected from the developing boundary layer. Therefore a plume is caused which eventually rises away from the boundary layer and, in this case, is advected to the right by the overall flow field generated by the hot surface. A very similar situation is shown in Fig. 10 where a snapshot of a simulation by Wooding et al. (1997) is given. Their situation is a model of an evaporating solar pond where there is a high solute concentration on the left hand two-thirds of the upper surface, and where evaporation causes fluid to leave the system to form a suction surface. The systems studied by Rees and Bassom (1993) and Wooding et al. (1997) would have been mathematically identical without the suction surface. Wooding et al. (1997) attribute this starting plume to a strong perturbation caused by high horizontal density gradients near the leading edge.

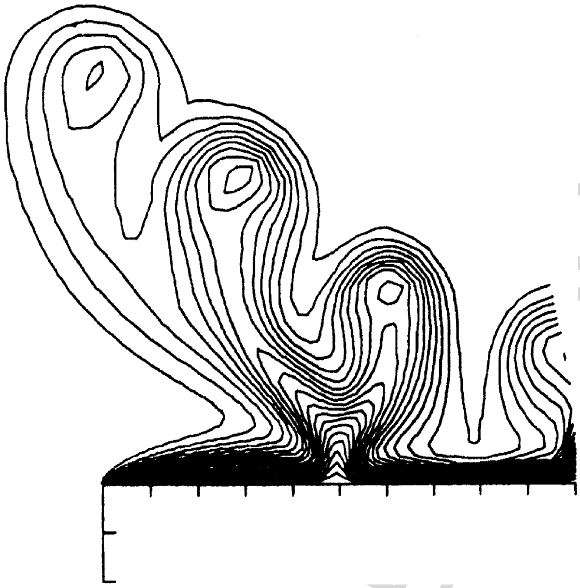

Fig. 9 Depicting the complex plume generated near the leading edge of a suddenly heated semi-infinite surface (Rees and Bassom 1993)

Fig. 10 Depicting the complex plume generated near the leading edge of a suddenly salted semi-infinite surface with suction (Wooding et al. 1997)

9 Conclusion

The study of the instability of unsteady boundary layers is an active topic. Much is known about the behaviour of the small-amplitude disturbances and the results obtained by Caltagirone (1980) and Selim and Rees (2007a) should be regarded as being the definitive instability criterion, at least for amplitude theory. There remain issues to resolve for the application of energy stability theory. No doubt it is possible to extend the linearised theory presented here to more complicated situations, such as systems with (i) discrete horizontal layers, (ii) non-Newtonian fluids and (iii) both heat and salt as diffusing species. It is likely that there could be some qualitative differences as compared with our standard problem. We think that it is possible to contrive layered situations where the neutral stability curve takes more exotic shapes, such as having two turning points—in such situations some disturbances could have two intervals of growth and three intervals of decay. Double diffusive convection offers parameter ranges where the primary mode at onset for the Darcy–Bénard problem is unsteady; similar ranges might make the development of an onset criterion for unsteady boundary layers somewhat problematical. Likewise viscoelastic fluids can admit highly oscillatory flows.

Of course many of these situations could be extended to the nonlinear domain, but we feel it would also be of some considerable interest to determine the nonlinear development of isolated disturbances.

However, of perhaps more importance is the fact that the basic state that we have studied does not have a linear profile because, in the Darcy–Bénard context, it is well-known that three dimensional convection often ensues in these situations. Therefore we think it highly likely that the preferred nonlinear flow will be three dimensional and possibly chaotic. The next step should therefore be the development of codes which are capable of producing computations such as those of Riaz et al. (2006) in three dimensions.

Finally, there already exist many studies where unsteady boundary layers are formed by boundary conditions which oscillate in time. Space has proved insufficient to give a review of this highly interesting topic.

Acknowledgment The first author would like to record his gratitude to Prof. Andrew Bassom who initiated his interest in studying boundary layer instabilities. He would also like to thank Dr. Aminreza Noghrehabadi who supplied all the calculations in Nouri-Borujerdi et al. (2007) while visiting the University of Bath.

References

Caltagirone J-P (1980) Stability of a saturated porous layer subject to a sudden rise in surface temperature: comparison between the linear and energy methods. Quart J Mech Appl Math 33:47–58.

Elder JW (1967) Transient convection in a porous medium. J Fluid Mech 27:609–623.

Elder JW (1968) The unstable thermal interface. J Fluid Mech 32:69–96.

Ennis-King JP, Paterson L (2005) Role of convective mixing in the long-term storage of carbon dioxide in deep saline formations. SPE J 10(3):349–356.

Ennis-King JP, Paterson L (2007) Coupling of geochemical reactions and convective mixing in the long-term geological storage of carbon dioxide. Int J Greenhouse Gas Control 1:86–93.

Ennis-King JP, Preston I, Paterson L (2005) Onset of convection in anisotropic porous media subject to a rapid change in boundary conditions. Phys Fluids 17:084107.1–084107.15.

Green T (1990) The momentary instability of a saturated porous layer with a time-dependent temperature distribution, and the most unstable disturbance. Water Resour Res 26:2015–2021.

Hassanzadeh H, Pooladi-Darvish M, Keith DW (2006) Stability of a fluid in a horizontal saturated porous layer: effect of non-linear concentration profile, initial, and boundary conditions. Transp Porous Med 65:193–211.

Horton CW, Rogers RT (1945) Convection currents in a porous medium. J Appl Phys 16:367–370.

Kim MC, Kim S (2005) Onset of convective instability in a fluid-saturated porous layer subjected to time-dependent heating. Int J Heat Mass Transfer 32:416–424.

Kim MC, Kim S, Choi CK (2002) Convective instability in fluid-saturated porous layer under uniform volumetric heat sources. Int Comm Heat Mass Transfer 29:919–928.

Kim MC, Kim S, Chung BJ, Choi CK (2003) Convective instability in a horizontal porous layer saturated with oil and a layer of gas underlying it. Int Comm Heat Mass Transfer 30:225–234.

Lapwood ER (1948) Convection of a fluid in a porous medium. Proc Camb Phil Soc 44:508–521.

Nouri-Borujerdi A, Noghrehabadi AR, Rees DAS (2007) The linear stability of a developing thermal front in a porous medium: the effect of local thermal nonequilibrium. Int J Heat Mass Transfer 50:3090–3099.

Rees DAS, Bassom AP (1993) The nonlinear nonparallel wave instability of free convection induced by a horizontal heated surface in fluid-saturated porous media. J Fluid Mech 253:267–296.

Riaz A, Hesse M, Tchelepi HA, Orr FM (2006) Onset of convection in a gravitationally unstable diffusive boundary layer in porous media. J Fluid Mech 548:87–111.

Selim A, Rees DAS (2007a) The stability of a developing thermal front in a porous medium. I. Linear theory. J Porous Med 10:1–15.

Selim A, Rees DAS (2007b) The stability of a developing thermal front in a porous medium. II. Nonlinear theory. J Porous Med 11:17–23.

AQ3 Selim A, Rees DAS (2007c) The stability of a developing thermal front in a porous medium. III. Secondary instabilities. (In preparation).

Tan K-K, Sam T, Jamaludin H (2003) The onset of transient convection in bottom heated porous media. Int J Heat Mass Transfer 46:2857–2873.

Wooding RA, Tyler SW, White I (1997) Convection in groundwater below an evaporating salt lake. I. Onset of instability. Water Resour Res 33:1199–1218.

Xu X, Chen S, Zhang D (2006) Convective stability analysis of the long-term storage of carbon dioxide in deep saline aquifers. Adv Water Resources 29:397–407.

Yoon DY, Choi CK (1989) Thermal convection in a saturated porous medium subjected to isothermal heating. Korean J Chem Eng 6:144–149.

Chapter-04

Query No.	Page No.	Line No.	Query
AQ1	94	06	we have renumbered the equation in accordance to maintain the sequential order. Is it Ok?.
AQ2	95	24	Rees and Selim (2007 a) is not listed in the reference list. Please provide.
AQ3	110	12	Please Update the reference Selim and Rees (2007 c).